All-printed diode operating at 1.6 GHz

Negar Abdollahi Sani, Mats Robertsson, Philip Cooper, Xin Wang, Magnus Svensson, Peter Andersson Ersman, Petronella Norberg, Marie Nilsson, David Nilsson, Xianjie Liu, Hjalmar Hesselbom, Laurent Akesso, Mats Fahlman, Xavier Crispin, Isak Engquist, Magnus Berggren and Goran Gustafsson

Original Publication:

Negar Abdollahi Sani, Mats Robertsson, Philip Cooper, Xin Wang, Magnus Svensson, Peter Andersson Ersman, Petronella Norberg, Marie Nilsson, David Nilsson, Xianjie Liu, Hjalmar Hesselbom, Laurent Akesso, Mats Fahlman, Xavier Crispin, Isak Engquist, Magnus Berggren and Goran Gustafsson, All-printed diode operating at 1.6 GHz, 2014, Proceedings of the National Academy of Sciences of the United States of America, (111), 33, 11943-11948.
http://dx.doi.org/10.1073/pnas.1401676111

An all-printed diode operating at 1.6 GHz

Negar Sani[a], Mats Robertsson[a], Philip Cooper[b], Xin Wang[c], Magnus Svensson[c], Peter Andersson Ersman[c], Petronella Norberg[c], Marie Nilsson[c], David Nilsson[c], Xianjie Liu[d], Hjalmar Hesselbom[e], Laurent Akesso[b], Mats Fahlman[d], Xavier Crispin[a], Isak Engquist[a], Magnus Berggren[a,c,1] and Göran Gustafsson[c,1]

[a] Linköping University, Department of Science and Technology, SE-601 74 Norrköping, Sweden
[b] De La Rue PLC , Research & Development , Overton, Hampshire RG25 3SE, United Kingdom
[c] Acreo AB, Printed Electronics, SE-602 22 Norrköping, Sweden
[d] Linköping University, Department of Physics, Chemistry and Biology, SE-581 83 Linköping, Sweden
[e] Hesselbom Innovation & Development H.B., Gymnasiev. 14, SE-14138 Huddinge, Sweden

[1] To whom correspondence may be addressed. E-mail: magnus.berggren@liu.se or goran.gustafsson@acreo.se

Keywords: Printed electronics, printed diode, flexible, UHF, silicon particle

Printed electronics are considered for wireless electronic tags and sensors within the future internet-of-things (IoT) concept. As a consequence of the low charge carrier mobility of present printable organic and inorganic semiconductors, the operational frequency of printed rectifiers is not high enough to enable direct communication and powering between mobile phones and printed e-tags. Here, we report an all-printed diode operating up to 1.6 GHz. The device, based on two stacked layers of Si and $NbSi_2$ particles, is manufactured on a flexible substrate at low temperature and in ambient atmosphere. The high charge carrier mobility of the Si micro-particles allows device operation to occur in the charge injection-limited regime. The asymmetry of the oxide layers in the resulting device stack leads to rectification of tunneling current. Printed diodes were combined with antennas and electrochromic displays to form an all-printed e-tag. The harvested signal from a GSM mobile phone was used to update the display. Our findings demonstrate a new communication pathway for printed electronics within IoT applications.

Significance Statement

Printed electronic labels and stickers are expected to define future outposts of the communication web, as remote sensors, detectors and as surveillance technology, within the Internet of things (IoT) concept. It is crucial to couple such technology with standard communication systems that commonly operate at GHz frequencies. To accomplish this, UHF rectification components manufactured in a low-temperature printing process are necessary. Here, we report an all-printed diode operating above 1 GHz, achieved using a combination of Si and $NbSi_2$ microparticles. The diode was integrated with a flexible antenna and a printed electrochromic display indicator to successfully demonstrate remote transfer of signal and power from a standard GSM phone to the resulting e-label.

Printed electronics is the use of conventional printing techniques for patterning materials (semiconductors, conductors, insulators) and manufacturing electronic components onto a wide range of flexible and organic substrates, such as paper, plastic foils and labels(1). A vision for printed electronics is to provide an electronic label (e-label) for the *internet-of-things* (IoT). For many targeted IoT applications, it would be of great importance if a smartphone operating in the UHF band (300 MHz to 3 GHz) could communicate directly with, or even power up, all-printed e-labels, and thereby serve as a communication base with e-labels as the outposts of the Internet. In pursuit of this goal, it is desirable to find low cost and low temperature manufacturing processes for ultra-high frequency (UHF) electronics to be compatible with organic carriers that are sensitive to high temperature.

One of the key electronic devices is the diode, which is widely used in a variety of circuits such as rectifiers, voltage multipliers and charge pumps, for applications such as AM radio and other types of receivers(2), and for energy harvesting circuits to extract energy from RF electromagnetic waves(3, 4). Printed circuits and devices such as diodes, capable of operation in the UHF band, will be a cornerstone in interfacing mobile telephony and printed functional objects, i.e. a “thing” in the IoT.

Until now, various diodes and transistors have been printed using either organic(5-10) or inorganic(11-24) semiconductors. Organic semiconductors are promising candidates for printed electronics due to their solution processability, which enables printing manufacturing of devices and circuits in an all-in-line production scheme. The charge carrier mobility of organic semiconductor thin films is directly related to the resulting operating frequency of the diode(25). High charge carrier mobility up to(10) 9.0 $cm^2V^{-1}s^{-1}$ has been obtained for highly crystalline organic semiconductor films created via a vacuum deposition technique. Following the demonstration of a pentacene-based rectifier operating in the high frequency range (~50 MHz)(25), only a few studies have reported on the potential of organic diodes for UHF applications. However, all of these require vacuum deposition techniques: organic PIN diode with a cut-off frequency of 100 MHz(6), C_{60}-metal oxide diode with a cut-off frequency of 800

MHz(5) and pentacene diode operating up to 870 MHz(9). Charge carrier mobility values above 1 $cm^2V^{-1}s^{-1}$ are challenging to achieve via solution processing techniques. Utilization of printing techniques for the fabrication of organic diodes leads to many technical challenges including the loss of molecular order that is a prerequisite for high mobility. State-of-the-art printed organic diodes operate below 10 MHz(7).

In case of inorganic materials the cut-off frequency depends on the mobility and the concentration(11) of the charge carriers. Thus, another strategy for printed UHF electronics would be to consider conventional inorganic semiconductors comprising high mobility and carrier concentration and modify the processing method to make it compatible with low temperature processing and traditional printing techniques(13). One way to achieve this is to utilize nanoparticle semiconductor inks, a route which was successfully used to demonstrate fully printed rectennas, however presently limited to an operational frequency of 13.56 MHz(16). With advances in chemistry and nanotechnology, solution processed inorganic semiconductors are now available(23, 24). Using such materials, solution processed films can be prepared through coating or printing processes. However, in order to improve the conductivity they usually need drastic or even extreme thermal treatments (high temperature sintering or laser annealing), which are not compatible with flexible substrates such as PET and paper(12, 14, 15, 17-19, 26). One solution suggested for dealing with this problem is to fabricate the device on a high temperature tolerant substrate first and then transfer it onto a flexible substrate. PIN diodes with a cut-off frequency of 1.9 GHz(22) and transistors with a cut-off frequency of 2.04 GHz(21) on flexible substrates have been developed using this method. However, this technique involves several steps, some that are certainly too complicated and time consuming for being feasible and cost-compatible with industrial mass production processes. Yet another recent strategy involving inorganic semiconductors is a low temperature aqueous route for fabrication of TFTs on plastic, yielding an average mobility of 2.6 $cm^2V^{-1}s^{-1}$ (20). One of the major challenges remaining here is to control the doping level via low temperature chemical growth.

To the best of our knowledge, all-printed UHF devices, such as transistors and diodes, achieved on flexible substrates, have so far not been demonstrated. With such a technology at hand, direct communication and powering between a cellular phone and printed e-labels would become possible.

Here, we utilize silicon (Si) micro-particles (µPs) in an organic binder as a screen-printable semiconductor composite, which is sandwiched between electrodes to form a diode. This allows us to directly profit from the combination of the high charge carrier mobility of the Si-crystal bulk (up to 1400 $cm^2V^{-1}s^{-1}$ for undoped Si), and the ability to use conventional printing processes. As a consequence, the printed Si-diode on a flexible substrate operates up to 1.6 GHz, i.e., within the UHF range. In fact, the energy harvested from the antenna of a mobile phone working in the Global System for Mobile Communications (GSM) band, while making a call, can be rectified using our printed Si-diode to power a printed electrochromic polymer display. This demonstrates the first direct communication between an all-printed e-label and a cellular phone.

Results and Discussion

To successfully use the printed diode, based on Si µPs, in future IoT applications, a simple and high throughput manufacturing process is needed. This forces us to consider well-established production techniques that makes use of manufacturing steps performed at low temperatures, in the ambience of a traditional printing house and that are compatible with common flexible plastic and paper substrates. Moreover, for communication at very high frequencies for power and signal transfer, the Si-diode must possess a very fast response to a voltage pulse while a large current rectification ratio is not as crucial as it would be in applications such as active matrixes. Hence, tunnel diodes and Schottky diodes are more appropriate than p-n diodes, because of their advantages in high speed operation (27, 28).

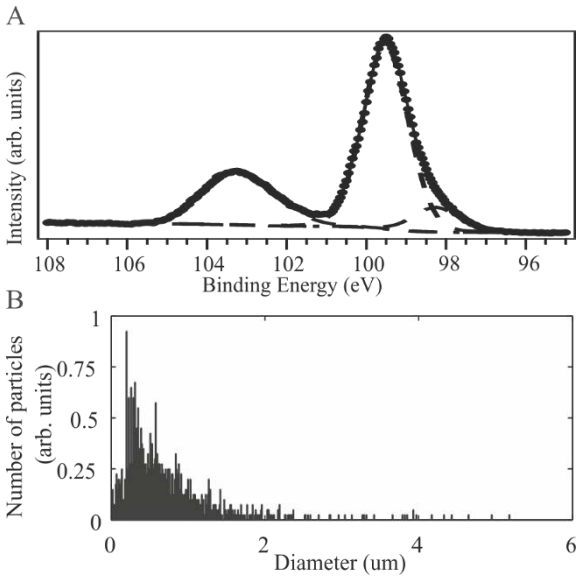

Fig. 1. Characterisation of Si µPs. (A) XPS measurements from the top surface of the Si/SU-8 layer. The low binding energy peak represents pure Si while the high-energy feature represents the SiO_2. By comparing the relative intensities of these two peaks and taking the photoelectron attenuation length into the account we estimate the oxide thickness d_{oxy} to 1.27 nm. (B) The size distribution of the Si µPs, measured using image analysis approach using SEM images from particles.

We used ball milling to crush a Si wafer into Si particles in air. Due to air exposure, the particles form a natural oxide shell layer. As long as the thickness of this insulating shell layer in a metal- insulator-semiconductor (MIS) diode is less than 50 Å, the device should behave as a Schottky diode(28). Films fabricated from the Si µPs in an organic binder were studied using X-ray photoelectron spectroscopy. The Si 2p core level was probed in order to obtain an estimate of the thickness of the SiO_2 outer shell covering the Si µPs, using the relative intensities of the Si 2p features (pure silicon, low binding energy peak) and silicon oxide (high binding energy peak), (see Fig. 1(A)). The part of the Si 2p spectrum related to pure silicon showed an asymmetry (small shoulder) on the low binding energy side and lacked the expected distinct spin-orbit splitting, which we attribute to charging effects since not all of the Si-particles in the film belong to a percolated network and thus will not maintain charge neutralization during the photoemission experiment. The Si 2p feature belonging to pure silicon was hence fitted (using a Shirley background) with two peaks and the silicon oxide feature with only one. The latter is the standard approach even for crystalline silicon films(29). Assuming random order of the Si µPs in the film, we can

exclude photoelectron diffraction effects and the oxide thickness d_{oxy} is then equal to 1.27 nm, following the procedure in Ref. 29 and using a photoelectron effective attenuation length λ_{oxy} = 2.96 nm for the native silicon oxide.

When considering the size of the Si particles, it is important to remember that the electron mobility decreases considerably with the size of the Si crystalline domains(1) because the wavefunction of the electron scatters at interfaces. Hence, the Si µPs are integrated in a polymer binder (SU8) to achieve a layer of less than 5 µm in thickness and ensure that the electronic charge carrier path between the two electrodes, sandwiching the Si layer, will pass through only one or just a few individual Si µPs. The measured size distribution of the Si particles is given in Fig. 1(B). To localize the current limitation of the diode to the Si particle/electrode interfaces, we choose n-doped crystalline Si, with a doping level of $\sim 10^{18}$ cm^{-3}, due to its high mobility and conductivity characteristics. The Si µPs are introduced along the surface of the SU8 precursor layer.

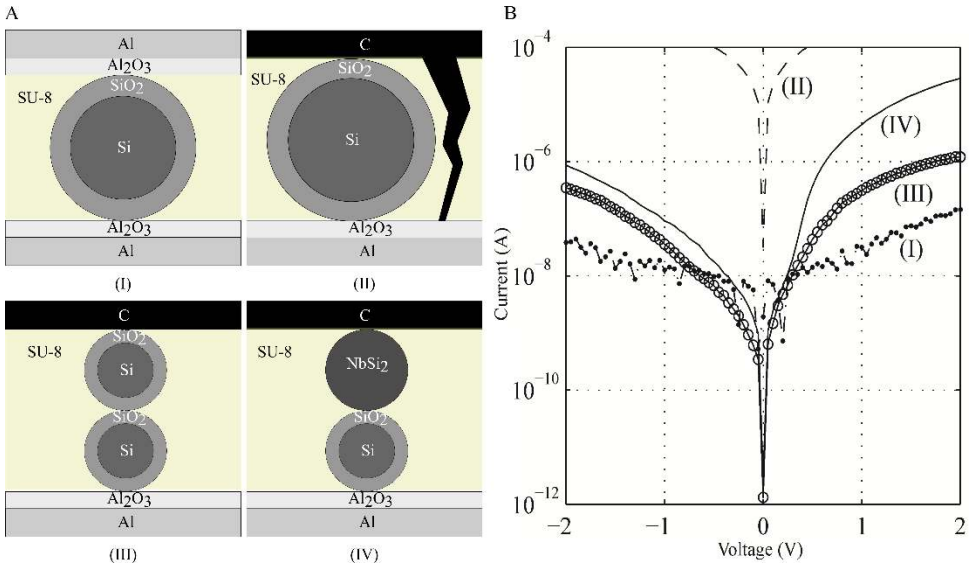

Fig. 2. Examining different device architectures. (A) Different device structures tested before designing the final structure of the device. (B) The I-V curves of the different device structures.

In the most simplified version, a diode device would be composed of n-Si µPs sandwiched between two electrodes (Fig. 2(A,I)). Compared to conventional MIS tunnel or Schottky diode, the geometry proposed is equivalent to two front-to-front connected MIS diodes. If the two MIS diodes are identical, very low current should pass through the structure in either forward or reverse bias. This is the case for a device composed of Si particles, with their natural oxide (thickness ~12.7 Å), in SU8 sandwiched between two aluminum electrodes (Fig. 2(A,I)). The measured I-V characteristics, see Fig. 2(B), for this device shows a low current level of around 10^{-7} A and practically no current rectification. In order to introduce current rectification (asymmetric device structure) in the I-V curve and to increase the current density, we replace the top Al/Al_2O_3 electrode with an oxide-free conductor. As a first candidate, we include conducting carbon that is easily printable in the form of a screen-printing paste (Fig. 2(A,II)). The top MIS contact diode includes only the thin silicon oxide layer (thickness ~12.7 Å), while the bottom contact diode combines both the silicon and the aluminum oxide layers (thickness 10-30 Å (30, 31)), coupled in series. However, since the carbon paste can penetrate through cracks in the Si-in-SU-8 layer, creating short circuits, the yield of this manufacturing process is rather low (31 %). Devices with high leakage currents, with charges running along the penetrating carbon contact directly to the aluminum bottom contact, all have a high current density (>10^{-4} A) and an ohmic current vs. voltage behavior without any rectification (dashed curve Fig. 2(B)). To suppress the possibility for the carbon top contact to penetrate the Si µP-in-SU8 layer, we added a second similar layer on top of the first layer after crosslinking. With this thicker Si µP-in-SU8 layer, short circuit effects were significantly reduced as indicated by the lower current level (III in Fig. 2(B)) but unfortunately the current density and rectification ratio are both too low for practical applications. We conclude from these experiments that the required additional layer should be an oxide-free conductor that is printable on top of the first Si-in-SU8 layer. Hence, we turn our attention to metal silicide, a family of highly conducting materials that are known to be resistant to oxidation(32, 33). We ground $NbSi_2$ powder into micro-particles, targeting a similar average µP size as for

the Si µPs (see Fig. S1), and then printed a $NbSi_2$-in-SU8 layer (less than 5 µm) on top of the Si-in-SU8 layer. The device was then finalized by printing a carbon paste top electrode (Fig. 2(A, IV)). Only 6% of these devices are short circuited, 50% of them have a rectification ratio lower than 10. Hence, 44% of the Carbon:$NbSi_2$-in-SU8: Si-in-SU8:Al diodes have a rectification >10 and of those, all devices show a cut-off frequency above 0.4 GHz. For a statistical comparison between the different structures shown in Fig. 2 II, III and IV, batches of 16 devices were manufactured for each of them. It is clear from these statistics that structure (IV) has the best yield and performance (for a summary, see Table S1). The rectification is measured at 1V; the amplitude required for demonstrating the concept of an e-label in this paper.

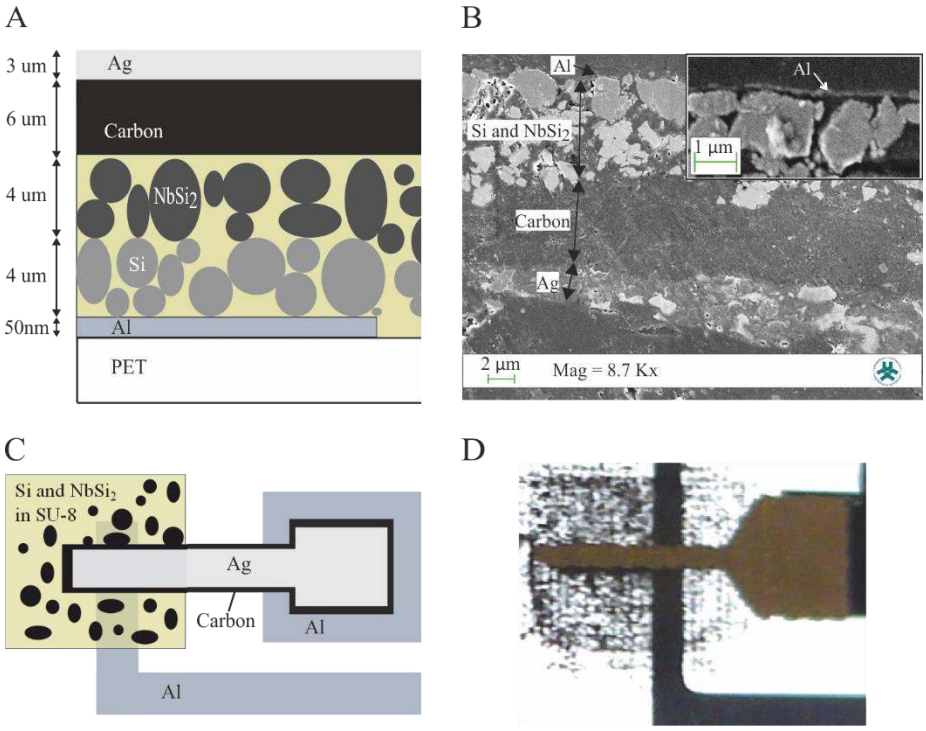

Fig. 3. Device structure (A) Schematic cross section of the device. (B) The SEM image of the cross section of the device where all the layers are clearly visible but the Al substrate. The inset shows a cross section of another device where the Al layer is visible. (C,D) Top view of the device.

The cross section of the final structure of the device is schematically illustrated in Fig. 3(A). The fabrication process starts with screen printing of dry Si particles on top of an inkjet-printed SU8 layer deposited on an Al substrate. The particles are then pressed down with a laminating machine to contact

the Al substrate through the binder. The dry $NbSi_2$ particles are screen-printed via a similar process. The SU8 binder is cross-linked at the end of each step. To finalize the diode, the carbon and Ag inks are subsequently screen-printed and cured. The reason for adding the carbon contact is to form a contact for the $NbSi_2$ particles, while the extra Ag layer is printed to further increase the conductivity of the top contact. An SEM cross section of the resulting device together with a top view is provided in Fig. 3(B-D).

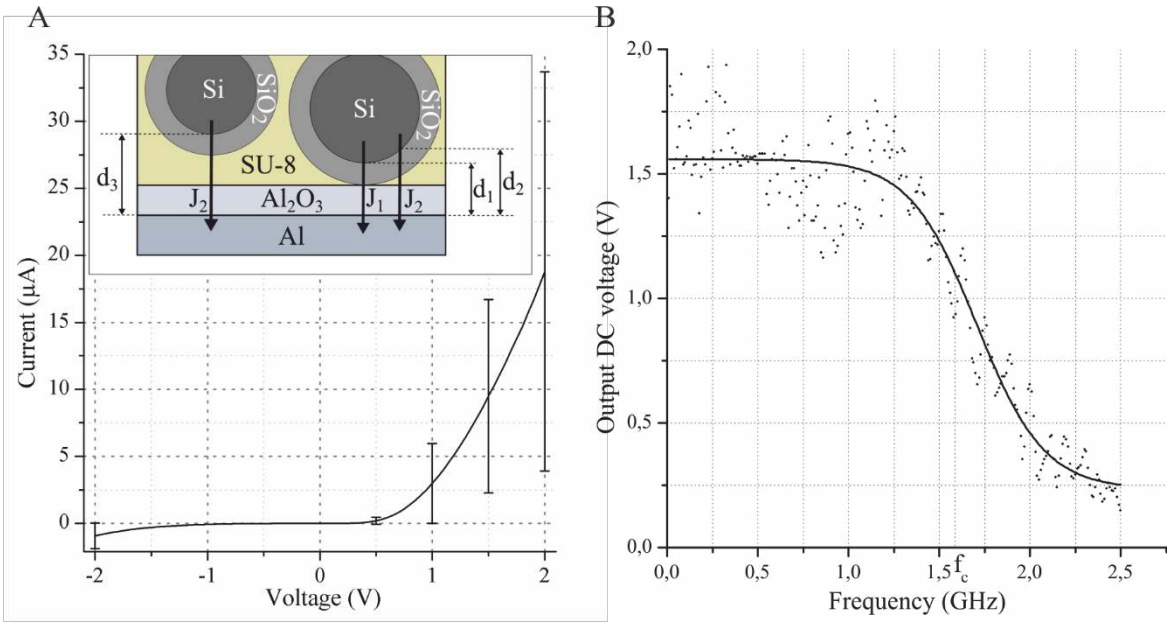

Fig. 4. DC characteristics and frequency response. (A) The average I-V curve based upon 16 representative devices. The error bars show the standard deviation and thus represent the voltage range needed to obtain a certain current level. Using a threshold of 3 μA, which we have defined as the on/off limit for the device, an average input voltage of 1V is needed to switch the diode on. The inset shows two different current mechanisms for different insulator thicknesses. (B) Frequency response of the device with an input power of 3 W.

The average I-V curve based upon 16 representative samples is shown in Fig. 4(A). A threshold current of 3 μA is defined as the limit between on and off states of the diode since this is the minimum current needed for switching an electrochromic display in a reasonably short time (10s of seconds). According to this definition the average turn-on voltage is about 1 V. The random distribution of particle sizes and distances and consequently the insulator thickness in the path of charges will result in some variation of the device characteristics, yielding a range of turn on voltages for different devices and a very low current amplitude for a percentage of the fabricated devices (that are discarded). The surface area of

the samples ranges from $2x10^4$ to $8x10^4$ μm^2. We report the resulting current amplitude rather than the current density, because the current in the device is not homogenously distributed over the whole surface area of the contacts and the μP-in-SU8 layers but rather follows a current filament dynamics. Therefore, the current level does not scale linearly with the surface area, at least not for the small variation of the active device areas we utilize in our experiments (see further Fig. S2). By increasing the area of the diodes, the risk for short-circuits due to the cracks or pinholes of the binder increases and also the operational bandwidth of the device decreases since the value of the parasitic capacitance is directly related to the surface area.

The average frequency response of a typical sample measured by applying a 3 W input signal is shown in Fig. 4(B). The estimated cut off frequency (half power point) of the device is about 1.6 GHz.

After discarding devices that exhibit low current characteristics or a poor current rectification ratio, 77 % of the remaining samples show a cut off frequency higher than 1 GHz, and 33% exhibit a cut off frequency of around 1.6 GHz. DC performance measurements have been repeated after two years on a batch of 30 devices. At 2 V where all the devices are certainly in “on” stage, 60% of the samples retain more than half of their initial current and 64% of them retain more than half of their initial rectification ratio. In order to investigate the reliability of the devices further, one of the devices was left running with 1 GHz input for one hour which is $3.6x10^{12}$ cycles. No decrease of the output signal was detected. Considering that these devices were not covered or encapsulated, the above data indicate a high reliability.

As shown above, the operational frequency of our printed diode reaches 1.6 GHz. The output signal of a mobile phone working in the GSM band, captured by a receiver antenna, could thus in principle be rectified by our diode to produce a DC voltage which can be used to power printed electronics, such as an electrochromic display indicator. To evaluate our printed diode in such an application a simple

integrated circuit was manufactured. The fully printed circuit was manufactured on a PET label substrate and includes an Al-foil antenna, our diode and an electrochromic polymer (EC) display(34), based on PEDOT:PSS (Fig. 5). The antenna is designed to capture the electromagnetic signal of a mobile phone working within the GSM band. The signal transmitted from the mobile phone, while making a call, is transferred to the antenna of the label and then rectified by the diode and used to power the switching of the EC display. The maximum power produced by the mobile phone reaches 2 W, but only a fraction of the emitted energy can be forwarded to the diode due to the path loss in wireless signal transfer. Despite this, the diode rectifies the signal and produces a DC voltage enough to switch the EC display. DC measurements show an average current of 19 μA at 2 V forward bias, and a rectification factor of about 100 at 1 V. The cut off frequency of our diodes is around 1.6 GHz and the transmission frequency of the GSM phone is located at 1.8 GHz. Despite this, there is still enough energy transmitted to the antenna and rectified by the printed diode to enable a swift switch of the printed EC display element. At optimum conditions it takes less than 10 s to switch the color of the EC display indicator from transparent (photo (A) in Fig. 5) to dark blue (photo (C) in Fig. 5). The full switching of the printed electrochromic display can be viewed in Movie s1.

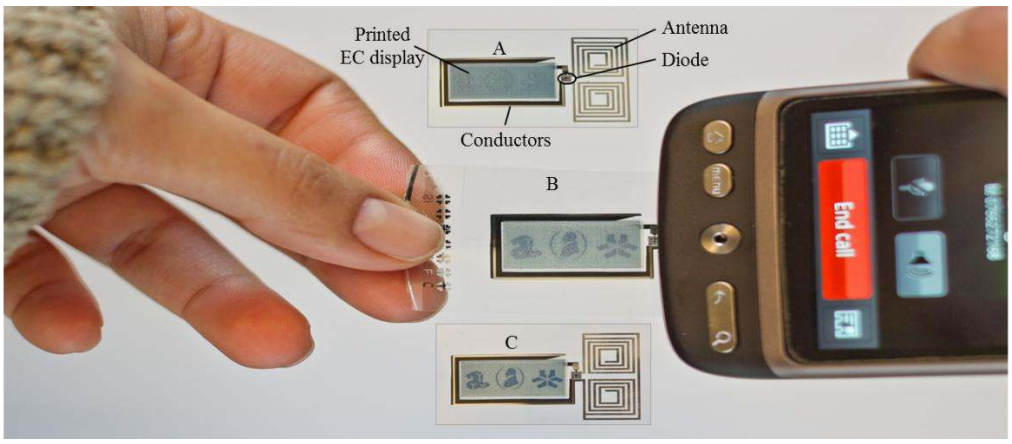

Fig. 5. Demonstration of e-label application (see Movie S1). (A) The antenna-diode-display circuit. (B) The mobile phone is held close to the antenna while making a call. The display starts to switch on. (C) The display is switched on after 10 s.

The semi-logarithmic I-V characteristics of the device, recorded at temperatures ranging from 150 K to 325 K, are displayed in Fig. 6(A). The UHF operation indicates that the rectification mechanism, more specifically the enhancement in current above 0.5 V in forward bias (Fig. 6(A)) is due to a very fast charge injection or displacement process, possibly tunneling(35). Note that the current below 0.7 V in forward bias and at all voltages in reverse bias is strongly dependent on the temperature. Conversely, above 0.7 V in forward bias, the current level is higher and is almost entirely temperature independent (see Fig. 6(A)). This is a feature that is characteristic for Fowler-Nordheim tunneling current(28).

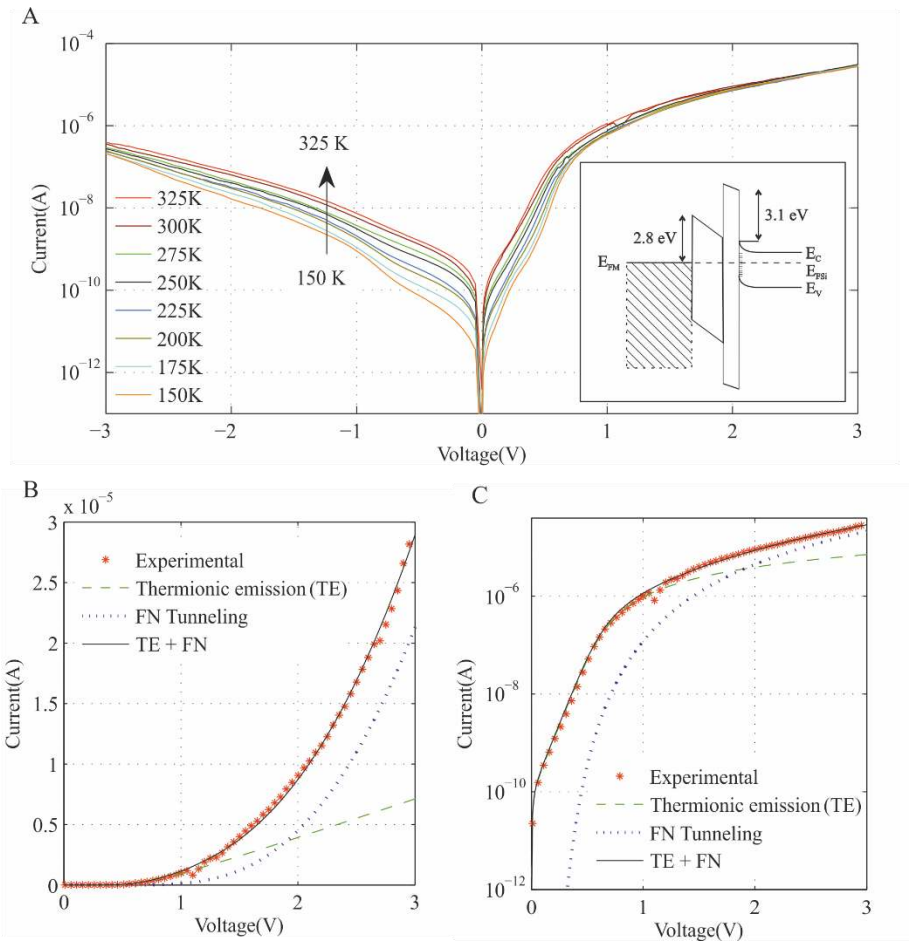

Fig. 6. Evaluation of the model. (A) Temperature dependence of the current-voltage characteristics in a semilogarithmic graph. The inset shows a simplistic band diagram of the Al-Si contact. As mentioned in the text, there will also most likely be trap states at the interface between the insulators, but these are not indicated in the figure due to lack of quantitative information. (B) The two current contributions (thermionic and tunnel currents) as well as the sum of those current contributions modeling the experimental data at T=300 K. (C) The two current contributions in a semi-logarithmic scale and the sum of those current contributions modeling the experimental data at T=300 K.

Since the oxide thickness between the Si particles and $NbSi_2$ particles is thinner than the one between the Si particles and the Al electrode, we believe that current is primarily limited by the energetics of the Al-Si contact. This kind of metal-insulator-semiconductor stack has been studied theoretically and experimentally with a precise control over the growth process and layer thicknesses in the past(36-43). However, the numerical values calculated for different parameters in previous studies cannot be directly used for modeling and comparison here, since our device has a much different structure that includes particles with random shapes, oxide layers with inhomogeneous properties and the organic binder. Although all the theory regarding modeling of semiconductor devices are based on planar contacts, we believe with some simplifications the behavior of the device can be approximated using classic semiconductor models. Due to the presence of surface states at the Si-SiO_2 interface, the Fermi level of Si is pinned and the barrier height cannot be calculated from the difference between the work function of the metal and the electron affinity of Si (as it would be in case of an intimate contact between metal and semiconductor (28)). A schematic illustration of the band diagram of the Al-Si contact is given in the inset of Fig. 6(A) incorporating values for the Si/SiO_2 and Al/Al_2O_3 barrier heights (3.1 eV and 2.8 eV, respectively)(44, 45). Applying a positive bias to Al lowers E_F of the metal as compared to Si and thus bends the semiconductor bands downwards causing the barrier height for the charges to decrease. If the thickness of the insulator layer is below 50 Å, direct tunneling may occur. The current in this case would follow the thermionic emission model multiplied by the tunneling probability factor. We assume that direct tunneling occurs at low voltages at the contact area between the Si particles and the soft Al film primarily across thin oxide paths since none of the other tunneling mechanisms can produce the current levels as high as we obtain in the device with this range of voltage. At higher voltages, the current can also pass through insulating regions with slightly larger Si-Al distance, as illustrated in the inset of Fig. 4(A), via other tunneling mechanisms mainly Fowler-Nordheim (FN) and Frenkel-Poole (FP)(46, 47). Moreover, in addition to the surface states at the interface between the semiconductor and the insulator, there are

other trap states in the insulator layers and at the interface between the insulators that can affect the current. However, based on the fact that the current is temperature-independent at high voltages, we believe that FN tunneling is the dominating mechanism. Therefore, a simplistic model based on direct tunneling at low voltages plus an FN tunneling that is added up at high voltages is presented here. Although other mechanisms such as FP tunneling can certainly be responsible for part of the current, especially in the intermediate voltage range, we refrain from attempting a model including all possible current mechanisms since the number of variables would be too large.

The current vs. voltage evolution for FN tunneling can be expressed as(28, 48):

$$I = C_1 V^2 \exp\left(\frac{-C_2}{V}\right) \qquad [1]$$

Where C_1 and C_2 are functions of the electron effective mass and the tunneling barrier. The Schottky model, based on the thermionic emission theory(28, 49), reproduces very well the experimental data for the low voltage region where FN current is negligible (the dashed line in Fig. 6(B,C)), but it deviates from the data as the voltage increases. A combination of thermionic emission and FN current (the dottedline in Fig. 6(B,C)) reproduces our measured I-V evolution at high voltages .

In the two-tunneling transport mechanism model, the total current-voltage relation of the device can be expressed as the linear combination of the tunnel assisted thermionic current (49, 50) (first term) and FN tunneling current (second term):

$$I = \alpha_1 T_t I_0 \exp\left(\frac{q(V-IR_s)}{nkT}\right)\left[1 - \exp\left(\frac{-q(V-IR_s)}{kT}\right)\right] + \alpha_2 C_1 V^2 \exp\left(\frac{-C_2}{V}\right) \qquad [2]$$

Where α_1 and α_2 are constants representing the relative contribution of each tunneling mechanism to the total current and I_0 is the reverse saturation current which is given by

$$I_0 = AA^*T^2 \exp\left(\frac{-q\Phi_b}{kT}\right) \qquad [3]$$

Where Φ_b is the barrier height, A is the surface area and A^* is the effective Richardson's constant. This model fully reproduces the temperature evolution of the I-V characteristics in forward bias (for plots, see Fig. S4).

The tunnel assisted thermionic forward bias current of a non-ideal diode is characterized by the series resistance R_s and the ideality factor n (k is the Boltzmann's constant, q is the electronic charge). In our case this current should be multiplied by a tunneling probability factor T_t. In order to extract the diode parameters, we started with determining the thermionic emission current parameters at the low voltage range, where the FN tunneling current is negligible. The procedure to extract those parameters is explained and outlined in detail in the supplementary information. The value of n, R_s and Φ_b at RT is found to be 2.9, 0.3 MΩ and 0.21 eV, respectively. The coefficient of the thermionic emission part of the current, T_tAA^* is calculated to be 3.88×10^{-12} AK^{-2}. Both barrier height and ideality factor are temperature dependent. As the temperature increases from 150 K to 325 K, the ideality factor decreases from 4.4 to 2.8 and the barrier height increases from 0.15 eV to 0.22 eV. Typically a low barrier height is expected in an Al/n-Si contact and the high values of the ideality factor are expected due to the existence of the oxide layer(51).

In summary, we demonstrated a printed diode with a vertical structure operating in the UHF band. DC measurements show an average current of 19 µA at 2 V forward bias, and a rectification factor of about 100 at 1 V. The lifetime of the device is more than 2 years. According to the measured frequency response of the diodes their cut off frequency is around 1.6 GHz, but they still have an output high enough to switch a printed organic display at the GSM frequency 1.8 GHz. These diodes can be used in a simple circuit to rectify an AC signal and convert it to DC, and since they can operate at GSM frequencies, it is possible to

simply use the signal of a mobile phone as the AC input signal source. The diode together with an antenna can be used to switch a printed organic display using the signal of an ordinary mobile phone.

Materials and Methods

The silicon powder is prepared using a Sb-doped silicon wafer with a resistivity of 0.01-0.02 Ω·cm. First a 4" wafer is broken into small pieces using a hammer. Then the parts are ball milled at 300 rpm for 16 hours in RETSCH PM 100 Planetary Ball Mill. The largest particles are separated away from the powder dispersed in acetone by gravity sedimentation in a cylinder tube. After this step, more acetone is added and the dispersion is centrifuged with MSE Mistral at 1000 rpm for 10 minutes. The suspension that contains the smallest particles is discarded and the bottom sedimentation is collected. The average size of the particles in the resulting powder is about 0.7 μm, but also includes particles with a size of up to 5 μm and lots of small particles below 0.5 μm; the smaller particles probably do not contribute to the current in the device but neither will cause any major performance degradation.

For fractioning of the niobium silicide powder, first 20 g niobium silicide (99.85% metals basis) powder is mixed with 8 g cyclohexanone and ball milled for 16 hours in RETSCH PM 100 Planetary Ball Mill. Afterwards gravitational sedimentation and centrifugation are used to separate the smallest particles away from the rest of the powder having a targeted average size similar to the silicon μPs.

The device is printed on top of an Al electrode on a PET substrate and connected to another Al electrode next to the first one via conductive carbon paste. The aluminum substrate pattern is prepared by photolithography from a 50 nm-thick aluminum evaporated on PET foil. The photoresist SU-8 2010 is diluted with isopropanol to 15% and screen printed on the aluminum electrode as a binder holding the silicon particles. The silicon particles are then screen printed on top of the SU-8 layer. The particles are pressed using a lamination machine with a pressure of 3 bar to make an intimate contact with the aluminum layer. The sample is then exposed to UV light for 1 min and heated at 95° C for 2 min to solidify

the SU-8. A layer of $NbSi_2$ particles with an average diameter size of 0.7 μm is screen printed onto a second layer of SU-8 on top of the first Si layer in the same manner. To finalize the device, carbon paste is screen printed on top of the $NbSi_2$-in-SU8 layer to provide a bridge to an aluminum contact pad used for probing. After curing the samples at 105° C for 5 min, a layer of Ag paste is screen printed on top of the carbon to further decrease the impedance of the bridge. The structure of the final device is illustrated in Fig. 3 (C,D). The surface area of the printed Si layer is $2x10^4$ to $8x10^4$ μm^2.

DC measurements of diode performance are made using an Agilent 4155B Semiconductor Parameter Analyser. For high frequency measurements a single harmonic signal is generated using an Agilent 8665B signal generator and applied to the device using a Cascade Microtech Air Coplanar Probe (ACP). The output signal from the device is then transferred to a low pass filter (LPF) using another ACP. The DC level of the output signal is measured using a Tektronix TDS 3034 oscilloscope with 1 MΩ load while the frequency of the input signal is swept between 10 MHz and 6 GHz. When the operational frequency reaches the HF and UHF range the system should be analyzed according to transmission line theory. One of the most important problems with this kind of measurement is the signal reflection at several points in the circuit where the impedances of the two sides of a junction are not matched. In our case the main cause of the signal reflection is the device itself, since it is a nonlinear device with an unknown and obviously frequency dependent impedance, while the rest of the circuit (cables and probes) has an impedance of 50 Ω. Hence, the output signal fluctuates as the frequency increases. Since it is impossible to completely eliminate the signal reflections in the wide range of frequency, we repeated the measurement with several combinations of 1 dB attenuators and RC loads (R = 50 Ω and C = 100 pF) in the junctions with highest reflections, trying to diminish the reflected signals. One of the measurement setups used for high frequency measurement is shown in Fig. S6. Despite the fact that the fluctuations in the V_{out} vs. frequency vary depending on the measurement setup, all of them show a similar trend which is interpreted as the actual frequency response of the diode using an averaging approach.

For characterization of the temperature dependence of the current the samples were probed in a cryogenic probe station and the I-V characteristic was measured using a Keithley 4200 semiconductor characterization system.

X-ray photoelectron spectroscopy, XPS, was carried out on ex-situ prepared samples using a monochromatized Al Kα (hν = 1486.6 eV) x-ray source and a Scienta-200 hemispherical analyzer. An electron flood gun was used to neutralize the sample during the XPS measurements due to the low conductivity of the sample. The reference energy position in the XPS spectra has been the C 1s peak, where the lowest binding energy of C 1s was set to 284.8 eV(52).

For characterizing the size distribution of the Si µPs, the particles were dispersed in HMDS to form a hydrophobic shell, preventing them from sticking to each other. The dispersion was then cast on an Al substrate and dried. A number of SEM images were taken and particle size analysis was performed for each image using the online tool SIMAGIS live for image analysis. The size distribution data of all the images was gathered to generate the final size distribution statistics.

Acknowledgements

The authors acknowledge VINNOVA (2012-01607), The European Regional Development Fund through Tillväxtverket (PEA-PPP) and The Knut and Alice Wallenberg foundation (Power Paper project, KAW 2011.0050). M.B. acknowledges The Önnesjö foundation, X.C. acknowledges the Advanced Functional Material program at Linköping University. X.L. acknowledges funding from The Swedish Research Council Linnaeus grant LiLi-NFM. The authors thank Lars Petterson and Duncan Platt, Acreo and Professor Robert Forchheimer, Dept. of Electrical Engineering (ISY), Linköping University for assistance in high frequency measurements and Anna Malmström for assistance in the lab and preparing the circuit layout.

References

1. **Sun, J., Zhang, B., & Katz, H. E. Materials for Printable, Transparent, and Low-Voltage Transistors *Advanced Functional Materials* 21, 29-45.**

2. **Carr, J. RF Components and Circuits (2002) *RF Components and Circuits* (Elsevier Science).**

3. **Nintanavongsa, P., Muncuk, U., Lewis, D. R., & Chowdhury, K. R. Design optimization and implementation for RF energy harvesting circuits (2012) *IEEE Journal on Emerging and Selected Topics in Circuits and Systems* 2, 24-33.**

4. **Jabbar, H., Song, Y. S., & Jeong, T. T. RF energy harvesting system and circuits for charging of mobile devices (2010) *IEEE Transactions on Consumer Electronics* 56, 247-253.**

5. **Im, D., Moon, H., Shin, M., Kim, J., & Yoo, S. Towards gigahertz operation: Ultrafast low turn-on organic diodes and rectifiers based on C60 and tungsten oxide (2011) *Advanced Materials* 23, 644-648.**

6. **Kleemann, H., Schumann, S., Jörges, U., Ellinger, F., Leo, K., & Lüssem, B. Organic pin-diodes approaching ultra-high-frequencies (2012) *Organic Electronics: physics, materials, applications* 13, 1114-1120.**

7. **Lilja, K. E., Bäcklund, T. G., Lupo, D., Hassinen, T., & Joutsenoja, T. Gravure printed organic rectifying diodes operating at high frequencies (2009) *Organic Electronics* 10, 1011-1014.**

8. **Park, S. K., Mourey, D. A., Subramanian, S., Anthony, J. E., & Jackson, T. N. High-mobility spin-cast organic thin film transistors (2008) *Applied Physics Letters* 93.**

9. **Steudel, S., Myny, K., Vicca, P., Cheyns, D., Genoe, J., & Heremans, P.Ultra-High Frequency rectification using organic diodes (2008) in *Electron Devices Meeting, 2008. IEDM 2008. IEEE International*, pp. 1-4.**

10. **Wang, M., Li, J., Zhao, G., Wu, Q., Huang, Y., Hu, W., Gao, X., Li, H., & Zhu, D. High-performance organic field-effect transistors based on single and large-area aligned crystalline microribbons of 6,13-dichloropentacene (2013) *Advanced Materials* 25, 2229-2233.**

11. **Champlin, K. S. & Eisenstein, G. CUTOFF FREQUENCY OF SUBMILLIMETER SCHOTTKY-BARRIER DIODES (1978) *IEEE Transactions on Microwave Theory and Techniques* MTT-26, 31-34.**

12. **Han, S., Dai, X., Loy, P., Lovaasen, J., Huether, J., Hoey, J. M., Wagner, A., Sandstrom, J., Bunzow, D., Swenson, O. F.*, et al.* Printed silicon as diode and FET materials - Preliminary results (2008) *Journal of Non-Crystalline Solids* 354, 2623-2626.**

13. **Johansson, C., Wang, X., & Robertsson, M. Printable rectifying device using Si-composite (2008) *Electronics Letters* 44, 53-55.**

14. **Kohno, A., Sameshima, T., Sano, N., Sekiya, M., & Hara, M. High performance poly-Si TFTs fabricated using pulsed laser annealing and remote plasma CVD with low temperature processing (1995) *IEEE Transactions on Electron Devices* 42, 251-257.**

15. **Mitzi, D. B., Kosbar, L. L., Murray, C. E., Copel, M., & Afzali, A. High-mobility ultrathin semiconducting films prepared by spin coating (2004) *Nature* 428, 299-303.**

16. **Park, H., Kang, H., Lee, Y., Park, Y., Noh, J., & Cho, G. Fully roll-to-roll gravure printed rectenna on plastic foils for wireless power transmission at 13.56MHz (2012) *Nanotechnology* 23.**

17. **Ridley, B. A., Nivi, B., & Jacobson, J. M. All-inorganic field effect transistors fabricated by printing (1999) *Science* 286, 746-749.**

18. **Sameshima, T., Usui, S., & Sekiya, M. XeCl EXCIMER LASER ANNEALING USED IN THE FABRICATION OF POLY-Si TFT'S' (1986) *Electron device letters* EDL-7, 276-278.**

19. **Shimoda, T., Matsuki, Y., Furusawa, M., Aoki, T., Yudasaka, I., Tanaka, H., Iwasawa, H., Wang, D., Miyasaka, M., & Takeuchi, Y. Solution-processed silicon films and transistors (2006) *Nature* 440, 783-786.**

20. **Young Hwan, H., Jin-Suk, S., Je Moon, Y., HyungJin, P., Shinhyuk, Y., Sang-Hee Ko, P., & Byeong-Soo, B. An 'aqueous route' for the fabrication of low-temperature-processable oxide flexible transparent thin-film transistors on plastic substrates (2013) *NPG Asia Materials* 5.**

21. **Yuan, H. C., Celler, G. K., & Ma, Z. 7.8-GHz flexible thin-film transistors on a low-temperature plastic substrate (2007) *Journal of Applied Physics* 102.**

22. **Yuan, H. C., Ma, Z., & Celler, G. K.Flexible RF/microwave switch-PIN diodes using single-crystal Si-nanomembranes (2007), pp. 1027-1030.**

23. **Zhang, X., Neiner, D., Wang, S., Louie, A. Y., & Kauzlarich, S. M. A new solution route to hydrogen-terminated silicon nanoparticles: Synthesis, functionalization and water stability (2007) *Nanotechnology* 18.**

24. **Härting, M., Zhang, J., Gamota, D. R., & Britton, D. T. Fully printed silicon field effect transistors (2009) *Applied Physics Letters* 94, -.**

25. **Steudel, S., Myny, K., Arkhipov, V., Deibel, G., De Vusser, S., Genoe, J., & Heremans, P. 50 MHz rectifier based on an organic diode (2005) *Nature Materials* 4, 597-600.**

26. **Zhou, H., Seo, J. H., Paskiewicz, D. M., Zhu, Y., Celler, G. K., Voyles, P. M., Zhou, W., Lagally, M. G., & Ma, Z. Fast flexible electronics with strained silicon nanomembranes (2013) *Scientific reports* 3, 1291.**

27. **Singh, J. Semiconductor devices: basic principles (2001) *Semiconductor devices: basic principles* (Wiley).**

28. **Sze, S. M. & Ng, K. K. Physics of Semiconductor Devices (2006) *Physics of Semiconductor Devices* (Wiley).**

29. **Lu, Z. H., McCaffrey, J. P., Brar, B., Wilk, G. D., Wallace, R. M., Feldman, L. C., & Tay, S. P. SiO2 film thickness metrology by x-ray photoelectron spectroscopy (1997) *Applied Physics Letters* 71, 2764-2766.**

30. **Hunter, M. S. & Fowle, P. Natural and Thermally Formed Oxide Films on Aluminum (1956) *Journal of The Electrochemical Society* 103, 482-485.**

31. Zähr, J., Oswald, S., Türpe, M., Ullrich, H. J., & Füssel, U. Characterisation of oxide and hydroxide layers on technical aluminum materials using XPS (2012) *Vacuum* 86, 1216-1219.

32. Horache, E., Fischer, J. E., & Van Der Spiegel, J. Niobium disilicide formation by rapid thermal processing: Resistivity-grain growth correlation and the role of native oxide (1990) *Journal of Applied Physics* 68, 4652-4655.

33. Kurokawa, K., Yamauchi, A., & Matsushita, S.Improvement of oxidation resistance of NbSi2 by addition of boron (2005), pp. 243-248.

34. www.paperdisplay.se.www.paperdisplay.se.

35. Chahal, P., Morris, F., & Frazier, G. Zero bias resonant tunnel Schottky contact diode for wide-band direct detection (2005) *IEEE Electron Device Letters* 26, 894-896.

36. Chattopadhyay, P. & Daw, A. N. On the current transport mechanism in a metal-insulator-semiconductor (MIS) diode (1986) *Solid State Electronics* 29, 555-560.

37. Iwata, S. & Ishizaka, A. Electron spectroscopic analysis of the SiO2/Si system and correlation with metal-oxide-semiconductor device characteristics (1996) *Journal of Applied Physics* 79, 6653-6713.

38. Card, H. C. & Rhoderick, E. H. Studies of tunnel MOS diodes I. Interface effects in silicon Schottky diodes (1971) *Journal of Physics D: Applied Physics* 4, 1589-1601.

39. Pananakakis, G., Kamarinos, G., El-Sayed, M., & Le Goascoz, V. Electrical characterization of Al-SiO2-Si (N-type) tunnel structures. Influence of LPCVD and LPO2 oxide growth technologies on the properties of the Si-SiO2 interface (1983) *Solid State Electronics* 26, 415-426.

40. Ng, K. K. & Card, H. C. ASYMMETRY IN THE SiO//2 TUNNELING BARRIERS TO ELECTRONS AND HOLES (1980) *Journal of Applied Physics* 51, 2153-2157.

41. Depas, M., Van Meirhaeghe, R. L., Laflère, W. H., & Cardon, F. Electrical characteristics of Al/SiO2/n-Si tunnel diodes with an oxide layer grown by rapid thermal oxidation (1994) *Solid State Electronics* 37, 433-441.

42. Altindal, Ş., Karadeniz, S., Tuğluoğlu, N., & Tataroglu, A. The role of interface states and series resistance on the I-V and C-V characteristics in Al/SnO2/p-Si Schottky diodes (2003) *Solid-State Electronics* 47, 1847-1854.

43. Cova, P., Singh, A., & Masut, R. A. A self-consistent technique for the analysis of the temperature dependence of current-voltage and capacitance-voltage characteristics of a tunnel metal-insulator-semiconductor structure (1997) *Journal of Applied Physics* 82, 5217-5226.

44. Aluguri, R., Das, S., Singha, R. K., & Ray, S. K. Size dependent charge storage characteristics of MBE grown Ge nanocrystals on surface oxidized Si (2013) *Current Applied Physics* 13, 12-17.

45. Derrie, J. & Commandré, M. SiO2 ultra thin film growth kinetics as investigated by surface techniques (1982) *Surface Science* 118, 32-46.

46. Frenkel, J. On Pre-Breakdown Phenomena in Insulators and Electronic Semi-Conductors (1938) *Physical Review* 54, 647-648.

47. **Jensen, K. L. Electron emission theory and its application: Fowler-Nordheim equation and beyond (2003) *Journal of Vacuum Science and Technology B: Microelectronics and Nanometer Structures* 21, 1528-1544.**

48. **Chiou, Y. L., Gambino, J. P., & Mohammad, M. Determination of the Fowler-Nordheim tunneling parameters from the Fowler-Nordheim plot (2001) *Solid-State Electronics* 45, 1787-1791.**

49. **Sze, S. M. Semiconductor Devices: Physics and Technology (2002) *Semiconductor Devices: Physics and Technology* (Wiley).**

50. **Sağlam, M., Ayyildiz, E., Gümüş, A., Türüt, A., Efeoğlu, H., & Tüzemen, S. Series resistance calculation for the Metal-Insulator-Semiconductor Schottky barrier diodes (1996) *Applied Physics A: Materials Science and Processing* 62, 269-273.**

51. **Kanbur, H., Altındal, Ş., & Tataroğlu, A. The effect of interface states, excess capacitance and series resistance in the Al/SiO2/p-Si Schottky diodes (2005) *Applied Surface Science* 252, 1732-1738.**

52. **Walther, F., Davydovskaya, P., Zürcher, S., Kaiser, M., Herberg, H., Gigler, A. M., & Stark, R. W. Stability of the hydrophilic behavior of oxygen plasma activated SU-8 (2007) *Journal of Micromechanics and Microengineering* 17, 524-531.**